The Implementation of Hybrid Observation Technique of Hilal (HOTOH)

A. L. A. M. Nasir
East Coast Environmental Research Institute (ESERI), Universiti Sultan Zainal Abidin (UniSZA)

R. Umar
East Coast Environmental Research Institute (ESERI), Universiti Sultan Zainal Abidin (UniSZA)

W. N. J. W. Yussof
Faculty of Computer Science and Mathematics (FSKM), Universiti Malaysia Terengganu (UMT)

N. Ahmad
Faculty of Science, Universiti Malaya (UM)

他

https://doi.org/10.5109/7323406

出版情報：Proceedings of International Exchange and Innovation Conference on Engineering & Sciences (IEICES). 10, pp.1174-1183, 2024-10-17. International Exchange and Innovation Conference on Engineering & Sciences
バージョン：

The Implementation of Hybrid Observation Technique of Hilal (HOTOH)

A. L. A. M. Nasir [1], R. Umar [1], , W. N. J. W. Yussof [2] , N. Ahmad [3] , A. N. Zulkeflee [4], N. H. Sabri [5], A. H. Kamarulzaman [1], N. A. Mahiddin[1]

[1] East Coast Environmental Research Institute (ESERI), Universiti Sultan Zainal Abidin (UniSZA), Kuala Nerus, 21300, Terengganu, Malaysia

[2] Faculty of Computer Science and Mathematics (FSKM), Universiti Malaysia Terengganu (UMT), Kuala Nerus, 21030, Terengganu, Malaysia

[3] Faculty of Science, Universiti Malaya (UM), 50603, Kuala Lumpur, Malaysia

[4] Department of Islamic Development Malaysia (JAKIM), 62100, Putrajaya, Malaysia

[5] Faculty of Science & Marine Environmental (FSSM), Universiti Malaysia Terengganu (UMT), Kuala Nerus, 21030, Terengganu, Malaysia

Corresponding author email: roslan@unisza.edu.my

Abstract: *In 2022, Malaysians were unexpectedly informed that Eid al-Fitr would be celebrated on 2nd May, disrupting plans based on the anticipated 3rd May date. This highlighted the need for better crescent moon sighting methods. This study aims to enhance new crescent detection accuracy through advanced image processing techniques using Contrast Limited Adaptive Histogram Equalization (CLAHE) for contrast enhancement, Bilateral Filter (BF) for denoising and Maximally Stable Extremal Regions (MSER) combined with Circular Hough Transform (CHT) for precise detection. The research showed significant improvements of using CLAHE for enhancing image contrast, BF for reducing the noise and MSER with CHT for ensuring accurate crescent detection. These techniques greatly improved crescent visibility and detection accuracy, preventing disruptions like the 2022 Eid announcement. This approach promises better predictability for future cultural and religious events.*

Keywords: New crescent moon; HOTOH; Image processing; Contrast enhancement; Object detection

1. INTRODUCTION

Hilal observation is pivotal in Islam as it determines the onset of crucial religious events such as Ramadan, Eid Al-Fitr (Shawwal) and the pilgrimage month of Dhu al-Hijjah. These events hold significant spiritual and communal importance for Muslims worldwide. The precise sighting of the new crescent moon marks the beginning of these periods, guiding millions in their observances and preparations. However, the accuracy of new crescent moon observation remains a challenge, primarily due to the inherent difficulties in visually distinguishing the faint crescent moon against the bright sky background.

The primary problem in new crescent moon observation is the low contrast between the new crescent moon and the sky background. The new moon is often very thin and faint, making it difficult for observers to spot, especially when atmospheric conditions are less than ideal. Light pollution significantly impacts the visibility of the new crescent moon, with better observations occurring under sky conditions measured between 16-22 mpsas [1]. Traditional methods rely heavily on human visual acuity and favorable weather, both of which are highly variable [2]. This challenge is compounded by the lack of real-time techniques designed specifically for new crescent moon detection, which further complicates the timely and accurate determination of important Islamic dates.

The social impact of inaccurate new crescent moon observation is profound. During Ramadan, the precise beginning and end of the fasting month are critical for the faithful. Mistimed announcements can lead to confusion and disrupt the fasting practices of entire communities. Similarly, the start of Shawwal, marked by Eid al-Fitr, is a time for celebration and communal gatherings. An abrupt or unexpected change in the date can disrupt social and economic activities, causing widespread inconvenience. Dhu al-Hijjah, the month of pilgrimage, is another period where precise timing is essential for millions of Muslims planning their journey to Mecca. Inaccurate new crescent moon sightings can lead to logistical challenges and affect the spiritual experiences of pilgrims.

To address these issues, this research proposes the use of advanced image processing techniques to enhance the visibility and precision of new crescent moon detection. By employing Contrast Limited Adaptive Histogram Equalization (CLAHE), the contrast of new crescent moon images can be significantly improved, making the faint crescent more distinguishable from the bright sky [3]. Additionally, the application of a Bilateral Filter helps to reduce noise while preserving important edges, ensuring the clarity of the new crescent moon [4]. For the object detection phase, combining Maximally Stable Extremal Regions (MSER) with Circular Hough Transform (CHT) techniques ensures high accuracy in identifying the new crescent moon's presence and shape.

The implementation of these advanced techniques can profoundly benefit the Muslim community. Accurate Hilal sightings ensure that Ramadan, Eid al-Fitr, and Dhu al-Hijjah begin and end on the correct dates, providing certainty and uniformity in observance. This reduces social and economic disruptions and allows for better logistical planning, particularly for the pilgrimage. By improving the accuracy of new crescent moon detection, this research not only enhances religious observances but also contributes to the overall harmony and spiritual well-being of Muslims worldwide.

2. METHODOLOGY

In this methodology, this research will propose the methodology that suitable for the new crescent moon sighting. Fig 1 shows the purpose of the methodology technique for new crescent moon visibility.

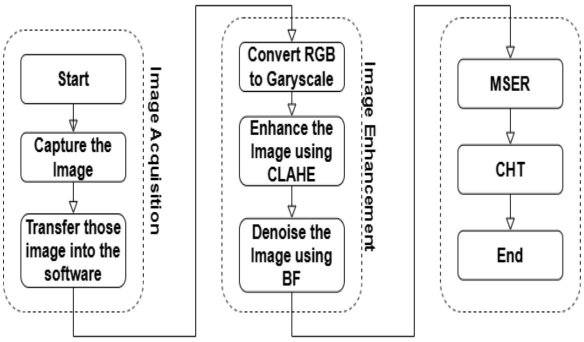

Fig. 1. Purpose of the methodology technique for new crescent moon visibility.

13 data was used to conduct this research, which is the data consist of a different moon sighting location in Malaysia to get the overview of the data of moonsighting in Malaysia. Teluk Kemang observatory was selected which is from west coast Malaysia, KUSZA observatory represent the east coast of Malaysia and the last one was Miri observatory which is from Borneo of Malaysia. Table 1 shows the 13 data that was used to conduct this research.

Table 1. 13 data were obtained from KUSZA, Teluk Kemang, and Miri

No	Observatory	Equipment	Date
1	Teluk Kemang	T-K1 Meade 8 + Canon DSLR	30 Sha'ban 1445H
2	KUSZA	Sky-Watcher 100ED Triplet + ZWOASI 1600MC	30 Sha'ban 1445H
3	Teluk Kemang	T-K4 WO 103 + ZWOASI 183MM	29 Rabi' al-Awwal 1444H
4	KUSZA	Sky-Watcher 72ED + ZWOASI 6200MM	29 Shawwal 1445H
5	Miri	RC6 + Canon EOS RA	30 Rajab 1444H
6	Teluk Kemang	William Optics GT 103 + ZWOASI 174MM	29 Ramadan 1445H
7	Teluk Kemang	William Optics 103 + Canon EOS 80D	30 Safar 1444H
8	Miri	Sky-Watcher Evostar 120ED + ZWO ASI 120MC	30 Sha'ban 1443H
9	Teluk Kemang	T-K3 WO 102 + ZWOASI 174MM	30 Safar 1445H
10	Teluk Kemang	William Optics 103 + Canon EOS 80D	30 Rabi' al-Awwal 1443H
11	Miri	Sky-Watcher ED Triplet 120MM + Canon EOS RA	30 Jumada al-Thani (Jamadil Akhir) 1443H
12	Teluk Kemang	Borg 101ED + Canon EOS 40D	30 Rabi' al-Awwal 1440H
13	KUSZA	FOT 86 + Sony a6500	30 Muharram 1445H

2.1 Image Acquisition

The data collection will begin by capturing the raw new crescent moon images using the appropriate telescopes and cameras. After that, those images will be transferred into the imaging software. This image will serve as the starting point for further image processing.

Fig. 2. Example of the raw image from KUSZA observatory on 30 Sha'ban 1445H.

2.2 Image Enhancement

In this process the image will undergo the 3 steps which are Grayscale conversion, CLAHE and BF.

2.2.1 Grayscale Conversion

The freshly acquired pictures of the crescent moon remained in color and represented using three-dimensional vectors, primarily the Red, Green, and Blue (RGB) color components. The order's dimensions are R×C×3, where R is the number of rows, C is the number of columns, and 3 symbolizes the three primary colors in RGB. [5]. The fundamental color image is encoded using 8 bits, resulting in a quantization level of 256. Therefore, if the red, green, and blue components each use 8 bits, their combination will use 24 bits in total, allowing for a total of 16,777,216 distinct colors [6]. The grayscale image is stored in 8 bits and has a total of 256 gray levels. Each pixel's intensity ranges from 0 to 255, with 0 representing black and 255 representing white [7].

The RGB image was transformed into a grayscale image in this study for multiple purposes. Initially, converting the image to grayscale can significantly decrease the amount of computational resources required for subsequent image processing techniques, such as enhancement. Furthermore, the utilization of single-component algorithms on color images can be streamlined by employing this conversion [5]. Ultimately, the grayscale image holds significance solely when the color image's brightness data is required. The conversion to grayscale can be achieved by utilizing the subsequent equation [7]:

$$I_G = (0.2989F_R + 0.5870F_G + 0.1140F_B) \tag{1}$$

F_R, F_G and F_B represent the intensity values of the red, green, and blue components, respectively. I_G corresponds to the intensity value equivalent to the gray level image within the RGB image. The coefficients (0.2989, 0.5870, and 0.1140) are the standard weights for converting RGB to grayscale, reflecting the human eye's sensitivity to different colors with green being the most sensitive and blue the least. Fig 3 displays the result of converting the raw image into grayscale. To differentiate between the new crescent moon and the sky in the images, it is necessary to utilize the luminosity of the image. Equation (1) is derived from the luminosity method and represents a computation of luminance, which is closely associated with lightness [8]. It calculates the average of the values, but incorporates a weighted average to consider human perception. Due to humans' heightened sensitivity to the color green compared to other colors, green is assigned the highest level of importance [9].

Fig. 3. From RGB to the Grayscale

2.2.2 CLAHE

The visibility of the new crescent moon in the image is restricted by the limited distinction between the object and the sky. Hence, the resolution to this issue necessitates the utilization of the CLAHE approach. This approach was first applied in medical imaging to assist the clear distinction of all contrast images crucial for clinical or research goals by the observer [10]. CLAHE is a more advanced version of the Adaptive Histogram Equalization (AHE) approach for increasing contrast. This most recent improved approach has proven useful for overcoming the limitations presented by conventional histogram equalization [11]. The selection of CLAHE was based on its proven ability to enhance the visibility of foggy images or videos [12]. The issue was nearly identical to the recently captured image of the crescent moon. The visibility of the new crescent moon was hindered by the presence of clouds in the sky [13]. The CLAHE approach incorporates HE into the context area. The contextual region is made up of each pixel from the original image positioned in the center of it. Following the clipping of the original histogram, the clipped pixels are evenly distributed throughout each gray level [14]. Afterwards, the CLAHE method enhances the contrast at each intensity level, resulting in a modified version of the regular histogram. This modification is constrained by a user-defined maximum value within the histogram [15]. The user-selectable maximum refers to the contrast limit, also known as the clip limit. The clip level will impact the amplification of noise and the enhancement of contrast [16]. The adaptive histogram clip (AHC) is a modified version of the contrast limiting technique that can also be utilized. AHC reduces excessive enhancement of image background regions by automatically adjusting clipping levels. The Rayleigh distribution is frequently used as an AHC and is known for generating a histogram with a bell-shaped curve. The distribution of Rayleigh serves as a continuous probability distribution in the field of probability theory and statistics. It is used to describe random variables that can only take non-negative values. [17,18]:

$$f(x;\alpha) = x/\alpha^2 \ \exp\left(-x^2/(2\alpha^2)\right), \boldsymbol{x} \geq 0 \tag{2}$$

Hence, the Cumulative Distribution Function (CDF) can be defined as the integral of the density function:

$$P(f) = 1 - \exp\left(-x^2/(2\alpha^2)\right) \tag{3}$$

The equation for CLAHE, which allows us to calculate the new gray levels is obtained from the inverse CDF as follows:

$$\mathrm{Rayleigh_g} = \mathrm{g}_{min} + [2(\alpha^2)\ In\ \left(\frac{1}{1-p(f)}\right)]^{0.5} \tag{4}$$

The Rayleigh distribution, used in probability theory and statistics for non-negative random variables is defined by its probability density function (Equation 2) and CDF (Equation 3), where x is the random variable and α is the scale parameter. In the context of CLAHE, equation 4 calculates new gray levels for image contrast enhancement by using the inverse CDF of the Rayleigh distribution, with g_{min} representing the minimum gray level and $P(f)$ the CDF value, thereby improving the image's visual quality by adjusting its contrast based on the Rayleigh distribution. Here, g_{min} represents the most minimal value among the pixels. In this study, the maximum threshold for clipping has been set as 0.1 for a high contrast image and 0.3 for a low contrast image. The selection of these values was aimed at maximizing the entropy value while minimizing the level of noise. Upon implementing the CLAHE technique on the grayscale image, the new crescent moon becomes distinctly discernible at the focal point of the image, as depicted in Fig 4. In order to demonstrate the superiority of the CLAHE technique in enhancing images, this study conducted a comparison with the contrast adjustment (CA) and standard histogram equalization (HE) techniques. The results of this comparison are illustrated in Fig 5. From the analysis of (b) and (c), it is apparent that both CA and HE techniques have a tendency to overexpose the input image by altering its brightness. It leads to the saturation of certain uniform regions in the output image with either very bright or very dark intensities [19]. Additionally, HE can occasionally result in increased noise levels, excessive enhancement, undesired visual distortions such as clipping or level saturation, and an imbalance among various elements of the output image [20].

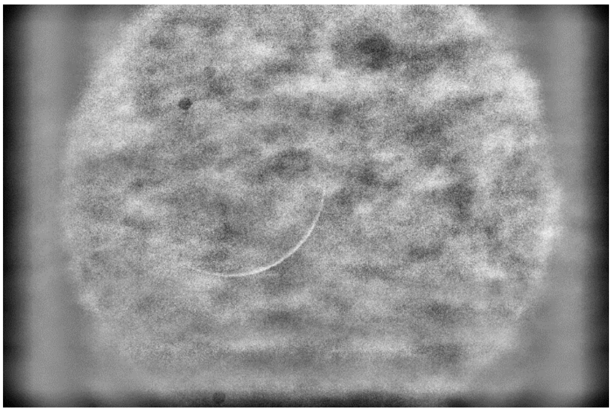

Fig.4. The new crescent moon in the image is more visible after using CLAHE technique

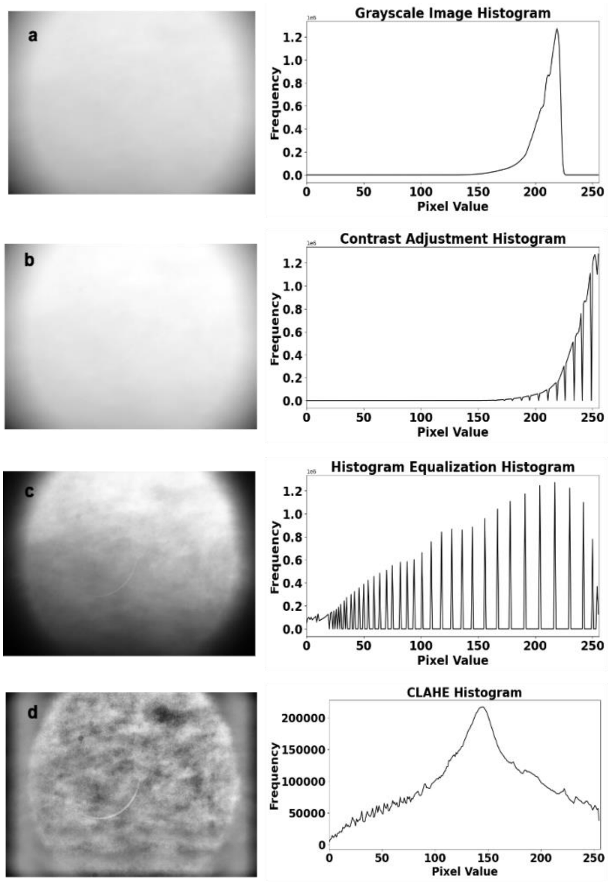

Fig. 5. Comparison between the (a) grayscale image, (b) contrast adjustment, (c) histogram equalization and (d) CLAHE and their histograms.

2.2.3 BF

Once the contrast enhancement process is finished, the bilateral filter will be used on the image to mitigate the issue of high noise levels. The technique, proposed by Tomasi and Manduchi in 1998 [21], the reason for choosing this filter is its non-linear nature, which effectively reduces noise while maintaining the integrity of the image's edge structures. The algorithm initiates by conducting an examination of a patch within the celestial area of the image. Next, the patch variance is then computed to approximate the noise variance. The bilateral filter is then applied to the image, followed by a specified amount of smoothing known as Degree of Smoothing (DoS). The DoS is set to be bigger in amplitude than the variability of the background noise. Thus, DoS was used in this work to minimize noise while conserving image quality. The bilateral filter is defined as follows [22]:

$$\mathrm{BF[I]_p} = \frac{1}{\mathrm{W_p}} \sum_{\mathrm{q} \epsilon \mathrm{S}} \mathrm{G}_{\sigma_\mathrm{s}}\left(||\mathrm{p}-\mathrm{q}||\right) \mathrm{G}_{\sigma_\mathrm{r}}\left(|\mathrm{I_p}-\mathrm{I_q}|\right) \mathrm{I_q} \qquad (5)$$

where, normalization factor ensures pixel weights sum up to 1.0:

$$W_\mathrm{p} = \sum_{\mathrm{q} \epsilon S} G_{\sigma_s}(||\mathrm{p}-\mathrm{q}||) G_{\sigma_\mathrm{r}}(|I_\mathrm{p} - I_\mathrm{q}|) \qquad (6)$$

In this equation (5), $BF[I]_p$ denotes the filtered intensity at pixel p, with W_p as the normalization factor ensuring that the weights sum to 1.0. The filter utilizes two Gaussian functions which is G_{σ_s}, the spatial Gaussian function, depends on the distance between pixels p and q, reducing the influence of far-away pixels and G_{σ_r}, the range Gaussian function, depends on the intensity difference between pixels p and q, reducing the impact of pixels with differing intensities. The normalization factor W_p given by Equation (6), represents a normalized weighted average. The parameters σ_s and σ_r determine the extent of spatial and range filtration applied to the image I, respectively. G_{σ_s} ensures that distant pixels have less influence, while G_{σ_r} ensures that pixels with different intensity values have reduced impact. Understanding that "range" relates to pixel values and "space" to pixel locations is crucial. This combined approach allows the bilateral filter to smooth images by averaging pixel intensities based on both spatial proximity and intensity similarity, effectively preserving edges while minimizing noise. Fig 6 displays the outcomes of the bilateral filter.

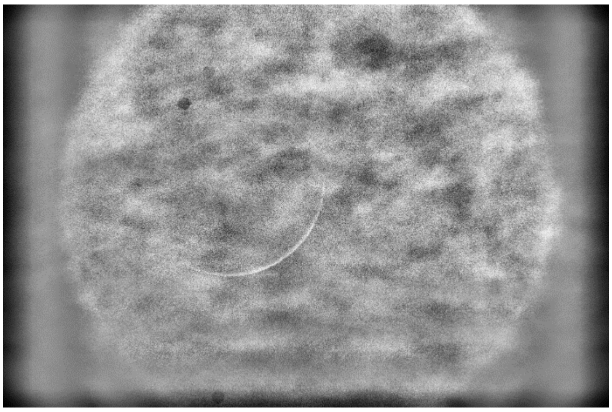

Fig. 6. Result after applying the BF

2.3 Image Detection

2.3.1 MSER

The enhanced image will then undergo the Maximally Stable Extremal Regions (MSER) technique to detect the recently formed crescent moon within the image. This technique was initially introduced by Matas [23] and has become one of the most widely used types of region detectors. Its popularity is from its exceptional repeatability and its compatibility with numerous other commonly utilized detectors. Due to their ability to handle a limited number of regions per image, they are highly suitable for large-scale image retrieval tasks [24]. MSERs are a collection of notable regions that are exclusively defined by the extreme property of an intensity function within the region and on its outer boundary [25]. MSERs can be defined as regions that present either a darker or brighter aspect compared to their surroundings and maintain their stability across a range of intensity function thresholds [26]. This method extracts consistent regions from an image by examining variations in the size of a connected component defined by applying a threshold to the image at a specific gray level, in relation to changes in its intensity [27]. The biggest advantages of MSERs were their minimum computational complexity and algorithmic structure, making them well-suited for hardware implementation. Furthermore, when faced with common image distortions, it is advantageous to have a reliable method for identifying essential image components that can be consistently repeated [28]. The maximally stable extremal region is formally defined as [29]:

$$\rho(R;\Delta) = \frac{|R_{+\Delta}| - |R_{-\Delta}|}{|R|} \tag{7}$$

The equation (7) is used to identify Maximally Stable Extremal Regions (MSER) in computer vision. An extremal region, or α-connectivity, is defined as a maximal connected component of a level set *S(i)*, where pixel intensities do not exceed *i*. In this context, *R* represents the original region, Δ is the change in intensity threshold, $R_{+\Delta}$ is the smallest extremal region containing *R*, with an intensity surpassing *R* by at least Δ, while $R_{-\Delta}$ is the largest extremal region contained within *R*, with an intensity at least Δ higher than *R*. The size of the original region is denoted by |*R*|. A region *R* is considered maximally stable when $\rho(R;\Delta)$ is minimized. The MSER algorithm begins by applying various thresholds to binarize the image, generating a series of binary images for each threshold. These regions are identified by their stability in size across different thresholds, making them robust and important features for image analysis. This method effectively highlights regions that maintain a consistent shape despite intensity variations, enhancing the detection and analysis of significant image features. This region is represented by the green area in Fig 7.

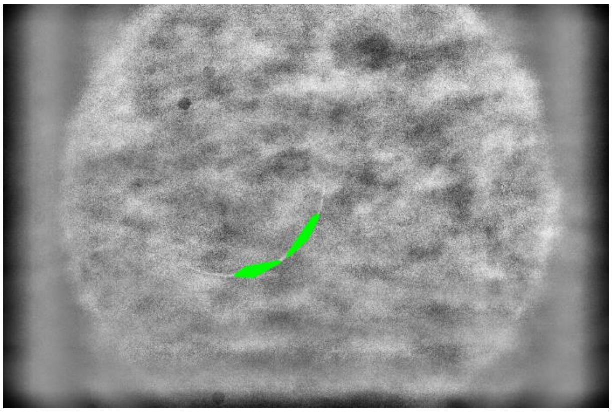

Fig. 7. The MSER result

2.3.2 CHT

The Circular Hough Transform (CHT), a method devised by Paul Hough in 1962, is used to identify circular objects in the image [30,31]. The Hough Transform operates by collecting votes for the geometric shape present at the edges [32,33]. The CHT procedure utilizes Equation (8).

$$r^2 = (x-a)^2 + (y-b)^2 \tag{8}$$

In the given equation (8), the variable *r* represents the radius, while *a* and *b* represent the coordinates of the circle's centre point and *x* and *y* represent the coordinates of any point on the circumference of the circle. The circular Hough transform approach described may be used to estimate the radius and centre point of a circular object [34,35]. The CHT algorithm is employed to capture the picture of the new crescent moon, which has an irregular circular shape [36]. The outputs of the CHT consist of a list that includes the coordinates of the centre point of the detected circle and the radius of the circle [37]. Fig. 8(a) displays the circle detection from the new crescent moon and Fig. 8(b) the output from the detection of the CHT in the real time image.

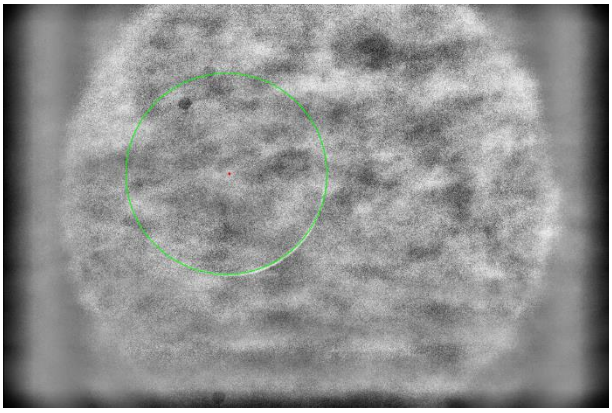

Fig. 8(a). Circle Detection Result at KUSZA Observatory

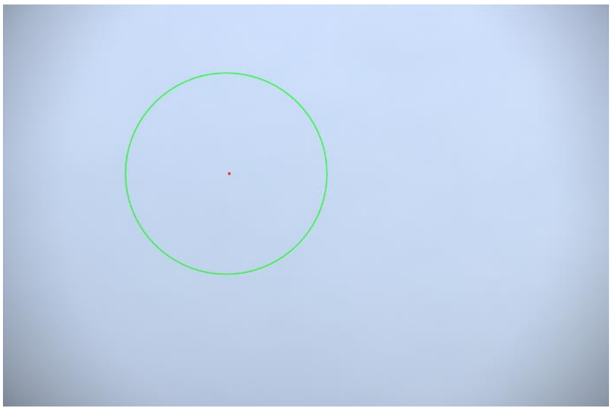

Fig.8(b). The output of the CHT in the real time image

3. RESULT AND DISCUSSION

In order to determine the effectiveness of the contrast enhancement technique, we compared the entropy value of the original image with those of the CA, HE, and CLAHE techniques. Entropy serves as a valuable metric for quantifying the amount of information contained within an image. An image with a high entropy value contains a greater amount of information, indicating that it possesses higher image quality [38]. Entropy, also referred to as information entropy Shannon's entropy is a quantitative measure that captures the level of uncertainty related to a source of information within the field of information theory. The equation can be precisely defined as follows [39]:

$$E(I) = -\sum_{k=0}^{L-1} p(k)\log_2(p(k)) \quad (9)$$

Where *I* represent the original image, *p(k)* represents the probability of value k occurring in image *I*, and $L=2^q$ represent the total number of distinct gray levels. *E(I)* represents the entropy of an image and should not be misconstrued as a mathematical expectation, as *I* is not a random variable. The entropy values for the tested image are displayed in Table 2. The entropy values of the CA and HE techniques are lower than those of the original image. This phenomenon is a result of overexposure that takes place when adjusting the brightness of the input image, as depicted in Fig 5(b) and (c), subsequently leading to a loss of image detail. The utilization of the CLAHE technique in this study yields a greater entropy value, signifying that this technique enhances the level of detail in the image, resulting in improved image quality. The lowest standard deviation value compared to other techniques also shows that CLAHE is the best technique for this study.

Table 2. Comparison of entropy values for various techniques used to test images.

Image	Original	CA	HE	CLAHE
1	3.9638	3.9475	3.7798	7.3401
2	5.3499	5.2782	5.2857	7.7944
3	5.4523	5.4523	5.4171	7.9762
4	5.1927	5.1925	5.0485	7.6556
5	4.6858	4.6858	4.6662	7.9774
6	5.8884	5.8884	5.8514	7.8443
7	6.8061	6.8051	6.6862	7.9909
8	2.7270	2.7270	2.7191	7.8502
9	4.6912	4.6912	4.6429	7.9087
10	5.4523	5.4523	5.4171	7.9762
11	3.5055	3.5055	3.4787	7.1997
12	7.0714	6.9094	7.0199	7.8343
13	5.8914	5.8906	5.8855	7.8880

Meanwhile, the image denoising technique's performance was assessed by comparing the peak signal to noise ratio (PSNR) values of contrast-enhanced and denoised image (CLAHE and BF, respectively). According to Table 3, reference pictures are grayscale images created by converting source photos. Contrast enhancement image (CLAHE) are images that have not yet been denoised, while denoised images (BF) have undergone the denoising procedure. PSNR is a metric that calculates the ratio of the greatest attainable signal strength to the power of the noise that reduces the quality of its representation. The signal represents original data, whereas noise refers to the flaws created by compression or distortion [40]. A higher PSNR value indicates superior picture quality. The PSNR between an example image and a test image, which are both equal size, is described as Hore & Ziou [41] as follows:

$$PSNR(f,g) = 10\log_{10}(255^2/\,MSE(f,g)) \quad (10)$$

Where,

$$MSE(f,g) = \frac{1}{MN}\sum_{i=1}^{M}\sum_{j=1}^{N}(f_{ij} - g_{ij})^2 \quad (11)$$

Equation (10) will measure the PSNR between the original image *f* and a reconstructed image *g*, where $PSNR(f,g)$ is expressed in decibels (dB) and provides a logarithmic scale to compare image quality. The key variable, $MSE(f,g)$, is the Mean Squared Error given by equation (11), which calculates the average squared differences between corresponding pixel values of the original image *f* and the reconstructed image *g*. Here, *M* and *N* represent the dimensions (height and width) of the images and f_{ij} and g_{ij} are the pixel values at the *i*-th row and *j*-th column of the original and reconstructed images. The PSNR equation uses a constant 255, the maximum possible pixel value for 8-bit images, to normalize the error measurement, ensuring that higher PSNR values indicate better image quality by quantifying the noise introduced during reconstruction. Table 3 presents a comparison of the PSNR values for both contrast-enhanced images using CLAHE technique and denoised images using the BF technique. It is clear that the denoised image exhibits a greater PSNR value in comparison to the contrast-enhanced image. These results demonstrate the efficacy of the BF technique in effectively reducing noise in the denoised image, thereby enhancing image quality.

Table 3. Comparison of PSNR values between contrast enhancement images (CLAHE) and denoised images (BF).

Grayscale	CLAHE	BF
1	27.7842	34.4185
2	27.8707	28.9254
3	27.9249	28.0294
4	27.8384	29.7161
5	27.7722	29.4146
6	27.8957	29.5516
7	27.8247	28.0507
8	27.4786	29.1989

Grayscale	CLAHE	BF
9	27.5101	29.7539
10	28.5781	29.8272
11	27.6527	31.9361
12	27.8808	28.3283
13	27.9787	30.2629

Furthermore, to evaluate the effectiveness of the object detection technique for MSER and the CHT, a comprehensive set metrics such as precision, recall, accuracy, F1 score, and false positive rate should be used [42]. Precision measures the proportion of true positive detections among all positive detections, while recall evaluates the proportion of true positive detections among all actual positive instances. Accuracy assesses the overall correctness of the detection system, combining both true positives and true negatives [43]. The F1 score provides a harmonic mean of precision and recall, offering a balanced evaluation metric. Lastly, the false positive rate quantifies the proportion of incorrect positive detections, which is crucial for understanding the system's reliability in real-world applications [44]. The precision are defined as follows [42]:

$$Precision = \frac{TP}{TP+FP} \quad (12)$$

$$Accuracy = \frac{TP+TN}{TP+TN+FP+FN} \quad (13)$$

$$Recall = \frac{TP}{TP+FN} \quad (14)$$

$$F1\ Score = 2 \times \frac{Precision \times Recall}{Precision + Recall} \quad (15)$$

and lastly, false positive rate [44]

$$FPR = \frac{FP}{FP+TN} \quad (16)$$

These equations are used to evaluate the performance of classification models, with key concepts including True Positives (TP), True Negatives (TN), False Positives (FP), and False Negatives (FN). Equation (12) measures the accuracy of positive predictions, where TP represents cases correctly identified as having the object, and FP indicates false prediction. Besides, equation (13), gauges overall correctness, including correctly identified negatives (TN) and missed detections (FN). Equation (14) assesses the model's ability to find all relevant instances. Meanwhile, equation (15) balances the precision and recall. Lastly, equation (16) shows the proportion of incorrect positive identifications among actual negatives.

Given the equations above, the definitions of TP, TN, FP, and FN are crucial for understanding the performance metrics of object detection models. TP represent cases where the model correctly predicts the presence of an object, thereby confirming its ability to identify true instances accurately. TN occur when the model correctly predicts the absence of an object, indicating its effectiveness in disregarding non-relevant data [45]. FP arise when the model incorrectly predicts the presence of an object that is not actually there, which can lead to false alarms and potential overestimation of the detection capabilities. On the other hand, FN happen when the model fails to detect an object that is present, pointing to a critical shortfall in the model’s detection ability. These definitions are integral to calculating precision, recall, accuracy, F1 score, and false positive rate, providing a comprehensive assessment of the model's performance and reliability in practical applications [46].

Based on the combined predictions for CHT, MSER and it combined method as shown in Table 4, the performance metrics reveal that combining these detection methods provides a balanced approach to new crescent moon detection. The combined method achieves an accuracy of 0.643, slightly higher than the 0.615 accuracy of either method alone (Fig 9). Precision remains perfect at 1.0 for the combined method, similar to MSER, indicating it eliminates false positives effectively. The recall of 0.615 for the combined method is an improvement over MSER’s 0.583 but slightly lower than CHT’s 0.667, reflecting a good balance in identifying true positives. The combined method’s F1 score of 0.761 is almost identical to CHT’s 0.762, demonstrating a well-rounded performance by balancing precision and recall. The false positive rate (FPR) for the combined method is 0.0, aligning with MSER’s performance and showing its effectiveness in avoiding incorrect positive predictions. This combination leverages the strengths of both methods, ensuring high precision while also improving recall over MSER alone. In practical terms, the combined method is highly reliable for confirming the presence of the moon due to its high precision and balanced recall. It is suitable for applications where minimizing false positives is crucial without significantly compromising the detection of true positives. This approach offers a robust solution, providing a good balance between avoiding false positives and capturing true positives, making it an effective choice for new moon detection scenarios.

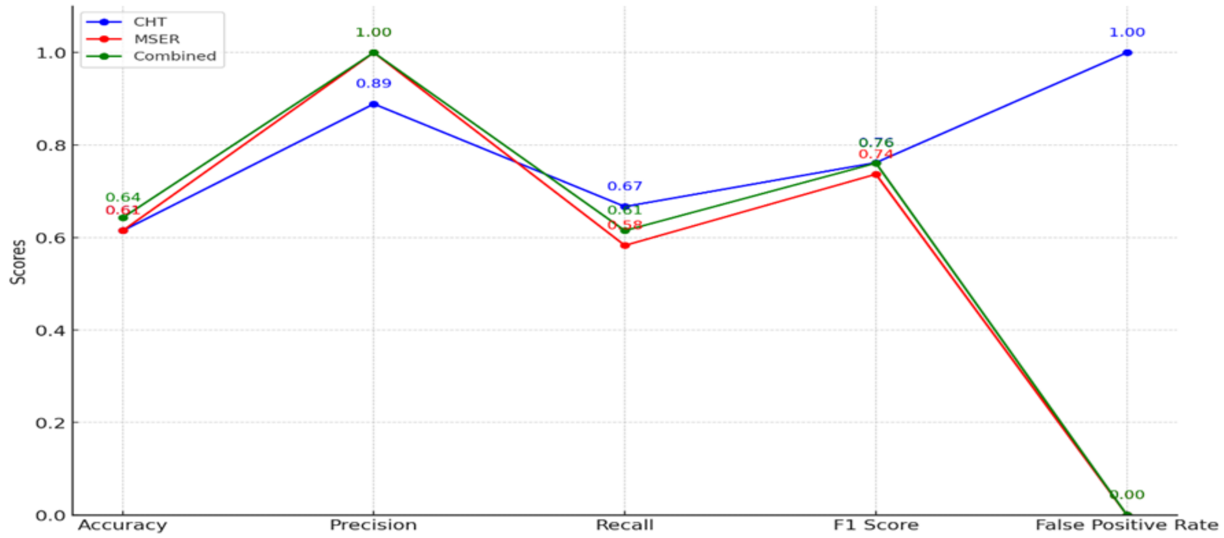

Fig. 9. The comparison of CHT, MSER and the combination of both detection technique in metrics line chart

Table 4. Combined true and false predictions for CHT, MSER and it combined method

Image Num	Ground Truth	CHT Prediction	CHT Type	MSER Prediction	MSER Type	Combined Prediction	Combined Type
1	Absent	Present	FP	Absent	TN	Absent	TN
2	Present	Absent	FN	Absent	FN	Absent	FN
3	Present	Absent	FN	Absent	FN	Absent	FN
4	Present	Present	TP	Present	TP	Present	TP
5	Present	Present	TP	Present	TP	Present	TP
6	Present	Present	TP	Present	TP	Present	TP
7	Present	Present	TP	Absent	FN	Present	TP
8	Present	Absent	FN	Absent	FN	Absent	FN
9	Present	Present	TP	Present	TP	Present	TP
10	Present	Present	TP	Present	TP	Present	TP
11	Present	Absent	FN	Absent	FN	Absent	FN
12	Present	Present	TP	Present	TP	Present	TP
13	Present	Present	TP	Present	TP	Present	TP

4. CONCLUSION

The proposed method for detecting the new crescent moon, which uses CLAHE for enhancing image quality, BF for reducing noise and combines MSER and CHT for detecting objects, offers numerous benefits that can positively impact society. This approach is crucial for improving the accuracy of astronomical observations and ensuring precise calendrical calculations, which are essential for cultural and religious practices that follow lunar calendars. By making moon sightings more reliable, communities can better align their events and rituals, ensuring everyone is on the same page. This method also highlights how advanced technology can solve traditional problems, encouraging collaboration across different fields and inspiring further innovation. In essence, this approach not only pushes the boundaries of scientific research but also helps preserve and support cultural traditions, making a real difference in both areas.

5. ACKNOWLEDGMENT

The authors would like to extend our heartfelt gratitude to the Ministry of Higher Education (MOHE) of Malaysia for the funding of this research under the Fundamental Research Grant Scheme (FRGS)-FRGS/1/2023/STG07/UNISZA/02/1. Special thanks are dedicated to Electromagnetic Research Group (EMRG) for their assistance in this work.

6. REFERENCE

[1] Shariff, N., Hamidi, Z., & Faid, M. S. (2017). The impact of light pollution on Islamic new moon (hilal) observation. *International Journal of Sustainable Lighting*, *19*(1), 10-14.

[2] Rashed, M. (2020). The circumstances controlling visibility of the Hijri lunar months. *International Journal of Advancements in Technology*, 1-1.

[3] Yussof, W. N. J. H. W., Man, M., Umar, R., Zulkeflee, A., Awalludin, E. A., & Ahmad, N. (2022). Enhancing Moon Crescent Visibility Using Contrast-Limited Adaptive Histogram Equalization and Bilateral Filtering Techniques. Journal of Telecommunictions Information Technology, 1(2022), 3-13.

[4] Cook, A. (2012). Lunar Observing Techniques. , 9-23.

[5] Dhal, K.G., Ray, S., Das, A., Fister, Jr., I., Das, S., 2019. Decolorization of digital pathology images: A comparative study. In: Computer Science Research Conference, Vol. 57.

[6] Saravanan, C., 2010. Color image to grayscale image conversion. In: 2010 Second International

Conference on Computer Engineering and Applications, Vol. 2. IEEE, pp. 196–199.
[7] Kumar, T., Verma, K., 2010. A theory based on conversion of RGB image to gray image. Int. J. Comput. Appl. 7 (2), 7–10.
[8] Bala, R., Braun, K.M., 2003. Color-to-grayscale conversion to maintain discrim inability. In: Color Imaging IX: Processing, Hardcopy, and Applications, Vol. 5293. SPIE, pp. 196–202.
[9] Kumar, R.V., Raju, K.P., Kumar, L.R., Kumar, M., 2016. Gray level to RGB using YcbCr color space technique. Int. J. Comput. Appl 147, 25–28.
[10] Pizer, S.M., Amburn, E.P., Austin, J.D., Cromartie, R., Geselowitz, A., Greer, T., ter Haar Romeny, B., Zimmerman, J.B., Zuiderveld, K., 1987. Adaptive histogram equalization and its variations. Comput. Vis. Graph. Image Process. 39 (3), 355–368.
[11] Zuiderveld, K., 1994. Contrast limited adaptive histogram equalization. In: Graphics Gems IV. Academic Press Professional, Inc., USA, pp. 474–485.
[12] Yadav, G., Maheshwari, S., Agarwal, A., 2014. Contrast limited adaptive histogram equalization based enhancement for real time video system. In: 2014 International Conference on Advances in Computing, Communications and Informatics (ICACCI). IEEE, pp. 2392–2397.
[13] Umar, R., Mat Jusoh, A.J., Mohd Nawawi, M.S.A., 2015. Pencerapan anak bulan Menggunakan optik dan radio. In: International Seminar on Al- Quran in Contemporary Society. UNISZA, pp. 108–121.
[14] Xu, Z., Liu, X., Chen, X., 2009. Fog removal from video sequences using contrast limited adaptive histogram equalization. In: 2009 International Conference on Computational Intelligence and Software Engineering. IEEE, pp. 1–4.
[15] Pizer, S., Johnston, R., Ericksen, J., Yankaskas, B., Muller, K., 1990. Contrast-limited adaptive histogram equalization: speed and effectiveness. In: [1990] Proceed ings of the First Conference on Visualization in Biomedical Computing. pp. 337–345.
[16] Pour, A.M., Seyedarabi, H., Jahromi, S.H.A., Javadzadeh, A., 2020. Automatic de tection and monitoring of diabetic retinopathy using efficient convolutional neural networks and contrast limited adaptive histogram equalization. IEEE Access 8, 136668–136673.Computer Science Research Conference, Vol. 57.
[17] Hitam, M.S., Awalludin, E.A., Yussof, W.N.J.H.W., Bachok, Z., 2013. Mixture contrast limited adaptive histogram equalization for underwater image enhancement. In: 2013 International Conference on Computer Applications Technology (ICCAT). IEEE, pp. 1–5..
[18] Singh, B.B., Patel, S., 2017. Efficient medical image enhancement using CLAHE enhancement and wavelet fusion. Int. J. Comput. Appl. 167 (5), 0975–8887.
[19] Ibrahim, H., Kong, N.S.P., 2007. Brightness preserving dynamic histogram equal ization for image contrast enhancement. IEEE Trans. Consum. Electron. 53 (4), 1752–1758.
[20] Oktavianto, B., Purboyo, T.W., 2018. A study of histogram equalization techniques for image enhancement. Int. J. Appl. Eng. Res. 13 (2), 1165–1170.
[21] Zhang, B., Allebach, J.P., 2008. Adaptive bilateral filter for sharpness enhancement and noise removal. IEEE Trans. Image Process. 17 (5), 664–678.
[22] Paris, S., Kornprobst, P., Tumblin, J., Durand, F., 2009. Bilateral filtering: Theory and applications. Now Publishers Inc.
[23] Matas, J., Chum, O., Urban, M., Pajdla, T., 2004. Robust wide-baseline stereo from maximally stable extremal regions. Image Vis. Comput. 22 (10), 761–767.
[24] Nistér, D., Stewénius, H., 2008. Linear time maximally stable extremal regions. In: European Conference on Computer Vision. Springer, pp. 183–196.
[25] Donoser, M., Bischof, H., 2006. Efficient maximally stable extremal region (MSER) tracking. In: 2006 IEEE Computer Society Conference on Computer Vision and Pattern Recognition (CVPR’06), Vol. 1. Ieee, pp. 553–560.
[26] Forssén, P.-E., Lowe, D.G., 2007. Shape descriptors for maximally stable extremal regions. In: 2007 IEEE 11th International Conference on Computer Vision. IEEE, pp. 1–8.
[27] Kimmel, R., Zhang, C., Bronstein, A., Bronstein, M., 2011. Are MSER features really interesting? IEEE Trans. Pattern Anal. Mach. Intell. 33 (11), 2316–2320.
[28] Śluzek, A., 2016. Improving performances of MSER features in matching and retrieval tasks. In: European Conference on Computer Vision. Springer, pp. 759–770.
[29] Huang, L., Xia, T., Zhang, Y., Lin, S., 2011. Human skin detection in images by MSER analysis. In: 2011 18th IEEE International Conference on Image Processing. IEEE, pp. 1257–1260.
[30] Cherabit, N., Chelali, F. Z., & Djeradi, A. (2012). Circular hough transform for iris localization. Science and Technology, 2(5), 114-121.
[31] Maitra, D., Rajan, & Singh, N. (2015). Seismic data interpretation using hough transformation technique. 2015 Ist International Conference on Next Generation Computing Technologies (NGCT), 580-583.
[32] Duman, E., Kökver, Y., Unver, H., & Erdem, O. (2017). Automatic landmark detection through circular hough transform in cephalometric X-rays. 2017 10th International Conference on Electrical and Electronics Engineering (ELECO), 583-587..
[33] Davies, E. R. (2003). An analysis of the geometric distortions produced by median and related image processing filters. *Advances in Imaging and Electron Physics, 126*, 93-193.
[34] Pala, M. A., & Yıldız, M. Z. (2024). Improving cellular analysis throughput of lens-free holographic microscopy with circular Hough transform and convolutional neural networks. *Optics & Laser Technology*, *176*, 110920.
[35] Jayadev, P. G., & Bellary, S. (2024). IrisSeg-drunk: enhanced iris segmentation and classification of drunk individuals using Modified Circle Hough Transform. *Iran Journal of Computer Science*, *7*(1), 41-54.
[36] Smereka, M., & Dulęba, I. (2008). Circular object detection using a modified Hough transform. *Journal*

of Automation, Mobile Robotics & Intelligent Systems, *18*, 85-91.
[37] Rizon, M., Yazid, H., Saad, P., Yeon, A., Shakaff, M., Saad, A. R. M., Sugisaka, M., Yaacob, S., Mamat, M., & Karthigayan, M. (2005). Object detection using circular Hough transform. *American Journal of Applied Sciences*, *2*, 1606-1609.
[38] Xiong, J., Yu, D., Wang, Q., Shu, L., Cen, J., Liang, Q., Chen, H., Sun, B., 2021. Application of histogram equalization for image enhancement in corrosion areas. Shock Vib. 2021.
[39] Mello Román, J.C., Vázquez Noguera, J.L., Legal-Ayala, H., Pinto-Roa, D.P., Gomez Guerrero, S., García Torres, M., 2019. Entropy and contrast enhancement of infrared thermal images using the multiscale top-hat transform. Entropy 21 (3), 244.
[40] Sara, U., Akter, M., Uddin, M.S., 2019. Image quality assessment through FSIM, SSIM, MSE and PSNR—a comparative study. J. Comput. Commun. 7 (3), 8–18.
[41] Hore, A., Ziou, D., 2010. Image quality metrics: PSNR vs. SSIM. In: 2010 20th International Conference on Pattern Recognition. IEEE, pp. 2366–2369.
[42] Takahashi, K., Yamamoto, K., Kuchiba, A., & Koyama, T. (2021). Confidence interval for micro-averaged F1 and macro-averaged F1 scores. *Applied intelligence (Dordrecht, Netherlands)*, 52, 4961 - 4972.
[43] Williams, C. (2020). The Effect of Class Imbalance on Precision-Recall Curves. *Neural Computation*, 1-5.
[44] Oksuz, K., Cam, B., Akbas, E., & Kalkan, S. (2018). Localization Recall Precision (LRP): A New Performance Metric for Object Detection. , 521-537.
[45] Lipton, Z., Elkan, C., & Narayanaswamy, B. (2014). Thresholding Classifiers to Maximize F1 Score. *arXiv: Machine Learning*.
[46] Okoye, G., & Umeh, E. (2023). Predicting Functional Outcome After Ischemic Stroke Using Logistic Regression and Machine Learning Models. *Earthline Journal of Mathematical Sciences*.
[47] Zhou, J., Ding, Z., Du, G., Zhao, S., Furukawa, T., & Lu, K. (2022, October 20). The RFID electronic tag defect detection system based on YOLOv5 for industrial scenarios. *Proceedings of the 8th International Exchange and Innovation Conference on Engineering & Sciences (IEICES 2022)*, 8, 44-51. Interdisciplinary Graduate School of Engineering Sciences, Kyushu University.
[48] Shaqour, A., & Farzaneh, H. (2021, October 21). Analyzing the impacts of a deep-learning based day-ahead residential demand response model on the Jordanian power sector in winter season. *Proceedings of the 7th International Exchange and Innovation Conference on Engineering & Sciences (IEICES 2021)*, 7, 247-254. Interdisciplinary Graduate School of Engineering Sciences, Kyushu University.